



# Efficient degradation of chloroquine drug by electro-Fenton oxidation: Effects of operating conditions and degradation mechanism

Sondos Midassi <sup>a</sup>, Ahmed Bedoui <sup>a</sup>, Nasr Bensalah <sup>b,\*</sup>

<sup>a</sup> Department of Chemistry, Faculty of Sciences of Gabes, University of Gabes, Gabes, 6072, Tunisia

<sup>b</sup> Department of Chemistry and Earth Sciences, College of Arts and Science, Qatar University, PO Box 2713, Doha, Qatar

## HIGHLIGHTS

- Chloroquine, an antiviral drug, has the potential to be persistent pollutant in water.
- Effective H<sub>2</sub>O<sub>2</sub> generation was obtained by pairing carbon felt cathode and BDD anode.
- Electro-Fenton-BDD depleted chloroquine from water independently of operating conditions.
- Chloroquine degradation leads to the formation of aromatic intermediates and carboxylic acids.
- Electro-Fenton achieved the release of Cl<sup>-</sup> ions and conversion of organic nitrogen to NO<sub>3</sub><sup>-</sup> and NH<sub>4</sub><sup>+</sup>.

## ARTICLE INFO

### Article history:

Received 23 April 2020

Received in revised form

25 June 2020

Accepted 28 June 2020

Available online 10 July 2020

Handling Editor: Shane Snyder

### Keywords:

Chloroquine

Electro-fenton

H<sub>2</sub>O<sub>2</sub> generation

Boron-doped diamond

Hydroxyl radicals

## ABSTRACT

In this work, the degradation of chloroquine (CLQ), an antiviral and antimalarial drug, using electro-Fenton oxidation was investigated. Due to the importance of hydrogen peroxide (H<sub>2</sub>O<sub>2</sub>) generation during electro-Fenton oxidation, effects of pH, current density, molecular oxygen (O<sub>2</sub>) flow rate, and anode material on H<sub>2</sub>O<sub>2</sub> generation were evaluated. H<sub>2</sub>O<sub>2</sub> generation was enhanced by increasing the current density up to 60 mA/cm<sup>2</sup> and the O<sub>2</sub> flow rate up to 80 mL/min at pH 3.0 and using carbon felt cathode and boron-doped diamond (BDD) anode. Electro-Fenton-BDD oxidation achieved the total CLQ depletion and 92% total organic carbon (TOC) removal. Electro-Fenton-BDD oxidation was more effective than electro-Fenton-Pt and anodic oxidation using Pt and BDD anodes. The efficiency of CLQ depletion by electro-Fenton-BDD oxidation raises by increasing the current density and Fe<sup>2+</sup> dose; however it drops with the increase of pH and CLQ concentration. CLQ depletion follows a pseudo-first order kinetics in all the experiments. The identification of CLQ degradation intermediates by chromatography methods confirms the formation of 7-chloro-4-quinolinamine, oxamic, and oxalic acids. Quantitative amounts of chlorides, nitrates, and ammonium ions are released during electro-Fenton oxidation of CLQ. The high efficiency of electro-Fenton oxidation derives from the generation of hydroxyl radicals from the catalytic decomposition of H<sub>2</sub>O<sub>2</sub> by Fe<sup>2+</sup> in solution, and the electrogeneration of hydroxyl and sulfates radicals and other strong oxidants (persulfates) from the oxidation of the electrolyte at the surface BDD anode. Electro-Fenton oxidation has the potential to be an alternative method for treating wastewaters contaminated with CLQ and its derivatives.

© 2020 The Authors. Published by Elsevier Ltd. This is an open access article under the CC BY license (<http://creativecommons.org/licenses/by/4.0/>).

## 1. Introduction

Chloroquine (CLQ), a generic pharmaceutical drug, is recommended as the primary antimalarial prevention drug (Frosch et al., 2011; Lee et al., 2011; Price et al., 2014) and to treat diseases such as

amoebic dysentery (Singh et al., 2011, 2013), and rheumatism (lupus erythematosus) (Furst, 1996; Howard, 2007; Schrezenmeier and Dörner, 2020). Recently, national and international health organizations permitted the treatment of Coronavirus (COVID-19) in certain hospitalized patients by chloroquine (Cortegiani et al., 2020; Devaux et al., 2020; J. Gao et al., 2020). The emergency authorization use of antimalarial drugs including CLQ requires manufacturing this drug in larger scale to fight COVID-19 that infected millions of people in the planet within few months.

\* Corresponding author.

E-mail address: [nasr.bensalah@qu.edu.qa](mailto:nasr.bensalah@qu.edu.qa) (N. Bensalah).

Accordingly, large quantities of wastewaters contaminated with CLQ will be discharged into the environment. CLQ has high potential to being persistent, bioaccumulate, and transfer to living organisms in intensified toxic forms owing to its antiviral and antibacterial characteristics. The high risks of natural water contamination due to the large production and utilization of CLQ, necessitates more attention to limit its hazardous effects on human health and environment (ozone depleting substance, bioaccumulation, and persistence).

Few are the studies reported in literature about the degradation and fate of CLQ in water (Ahmad et al., 2016; Coelho et al., 2017; Doddaga; Peddakonda, 2013; Karim et al., 1994; Nord et al., 1991). Mostly, the studies cited in literature have been focused on the photochemical stability of HCQ in water and none of them investigated its removal from water. Coelho et al. (2017) investigated the forced degradation of CLQ in water by alkaline hydrolysis and chemical oxidation with diluted  $\text{H}_2\text{O}_2$ . The degradation of CLQ into simpler molecules was confirmed by high performance liquid chromatography (HPLC) (Coelho et al., 2017); however, the degradation products themselves can cause substantial environmental concerns due to their high toxicity and bioresistance (Ahmad et al., 2016; Doddaga; Peddakonda, 2013). The growing interests on CLQ to prevent a diversity of diseases including the new quickly spreading COVID-19, requires an urgent search for an efficient water treatment method having the ability to destroy this micro-pollutant and remove it from wastewaters or at least convert it into less harmful and easy biodegrade substances before its discharge into the environment.

Advanced oxidation processes (AOPs) have attracted an increasing interest to substitute and complement with the traditional wastewater treatment methods due their higher efficacy in destroying a myriad of organic pollutants in water (Asgar et al., 2015a; Boczkaj and Fernandes, 2017; Cheng et al., 2016; Deng and Zhao, 2015; Pignatello et al., 2006). The reasons are related to their competency to produce large quantities of powerful oxidizing radicals among them hydroxyl radicals ( $\text{HO}^\bullet$ ) (Kanakaraju et al., 2018; Miklos et al., 2018; Wang and Xu, 2012). Being unstable with short residence time (Gligorovski et al., 2015; Peralta et al., 2014; Xiang et al., 2011), these radical species react immediately in a non-selective mode with organic pollutants and convert them into harmless compounds and occasionally to valuable products (Badmus et al., 2018; Tayo et al., 2018; Vallejo et al., 2015). AOPs are based on redox reactions between oxidants and reductants in solution and/or combination of chemical reactants with physical activating methods (Cheng et al., 2016; Gągol et al., 2018). Particularly, AOPs based on chemical and photochemical decomposition of hydrogen peroxide ( $\text{H}_2\text{O}_2$ ) to produce  $\text{HO}^\bullet$  radicals have drawn more attention due to their high efficacy, cost-effectiveness, and possibility to scale up (Ahmed et al., 2011, 2009; Asghar et al., 2015b; Bensalah et al., 2018; Bokare and Choi, 2014; Pham et al., 2012). Fenton and Fenton-like (Babuponnusami and Muthukumar, 2014a; Jiang et al., 2010), photo-Fenton (Clarizia et al., 2017; Dbira et al., 2014), and electro-Fenton (Brillas and Martinez-Huitle, 2009; Hou et al., 2018) processes are among  $\text{H}_2\text{O}_2$ -based AOPs most investigated for water treatment in small- and large-scale applications.

In Fenton and photo-Fenton processes, the addition of desired amounts of  $\text{H}_2\text{O}_2$  as reactant is required among other things (pH control, addition of  $\text{Fe}^{2+}$  catalyst) (Asgar et al., 2015a; Babuponnusami and Muthukumar, 2014b), while in electro-Fenton process,  $\text{H}_2\text{O}_2$  is electrogenerated in situ from the cathodic reduction of molecular oxygen ( $\text{O}_2$ ) (Bensalah et al., 2013). The in situ electrogeneration of  $\text{H}_2\text{O}_2$  results in virtuous control of the oxidation, lessens the safety risks associated with the transport and storage of this hazardous and unstable chemical, and then reduces

the overall costs of the treatment. The electrodes' materials play a crucial role in the improvement of the effectiveness of electro-Fenton oxidation (El-Ghenymy et al., 2012; Guinea et al., 2010; Moreira et al., 2013; Pinheiro et al., 2019; Yang et al., 2017; Zhang et al., 2018). Especially, the kinetics and current efficiency of the production of  $\text{H}_2\text{O}_2$  from the electrochemical reduction of  $\text{O}_2$  at the surface of the cathode is extensively influenced by the cathode's material. Brillas et al. (2009) stated that Hg, C-graphite, carbon-PTFE  $\text{O}_2$  diffusion, carbon felt and others materials can reduce  $\text{O}_2$  into  $\text{H}_2\text{O}_2$  in water with high current efficiency. Carbon felt a 3D material, is a cost-effective cathode material for electro-Fenton oxidation (Gong et al., 2016; Huang Le et al., 2017; Yu et al., 2015, 2014). Furthermore, recent studies showed that pairing carbon felt cathode with boron doped diamond anode (BDD) could boost the efficacy of electro-Fenton oxidation (Borrás et al., 2013; El-Ghenymy et al., 2015; Ruiz et al., 2011). BDD anode is known by its capability to produce  $\text{HO}^\bullet$  radicals and other strong oxidants from the oxidation of the electrolyte (Bensalah et al., 2015; Groenen Serrano, 2018; Marselli et al., 2003; Michaud et al., 2003). The supplementary production of strong oxidants at BDD anode and the continuous generation of  $\text{H}_2\text{O}_2$  and regeneration of the catalyst ( $\text{Fe}^{2+}$ ) by electrochemical reduction of  $\text{O}_2$  and  $\text{Fe}^{3+}$  ions at the cathode offer to this type of AOP an outstanding effectiveness compared to other AOPs in the destruction of organic pollutants in water (Bensalah et al., 2015; Groenen Serrano, 2018; Marselli et al., 2003).

This work aims to investigate the degradation of CLQ in water by electro-Fenton oxidation using carbon felt as cathode material, and Pt and BDD as anode materials. The results will offer significant information needed in the future to depollute large quantities of wastewaters contaminated with CLQ drug and its metabolites especially this drug is adopted as the first treatment of COVID-19 by many health organizations. The electrogeneration of  $\text{H}_2\text{O}_2$  during electrolysis was investigated at different operating conditions. The degradation of CLQ by electro-Fenton oxidation under various conditions (pH, current density, CLQ concentration,  $\text{Fe}^{2+}$  concentration) was monitored by HPLC analysis and total organic carbon (TOC) measurement. The analysis of organic and inorganic intermediates and final products was conducted using HPLC and ion chromatography (IC).

## 2. Materials and methods

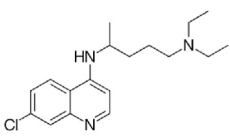
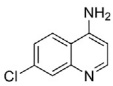
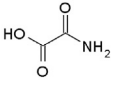
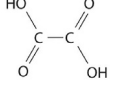
### 2.1. Chemicals

CLQ N4-(7-Chloro-4-quinolyl)-N1,N1-diethyl-1,4-pentanediamine Diphosphate (see Table 1) was purchased from VWR (with purity  $\geq 98\%$ ). 7-chloro-4-quinolinamine (4-Amino-7-chloroquinoline) (CQLA) was obtained from Sigma-Aldrich (see Table 1). Oxalic acid (OAA) (anhydrous,  $\geq 98.0$ ) and oxamic acid (OAMA) (anhydrous,  $\geq 97.0$ ) were received from VWR (see Table 1). 30% (by mass)  $\text{H}_2\text{O}_2$  solutions were purchased from VWR. Analytical grade  $\text{FeSO}_4 \cdot 7\text{H}_2\text{O}$ ,  $\text{Na}_2\text{SO}_3$ , and  $\text{Ti}(\text{SO}_4)_2$  were used as received from Sigma-Aldrich. The other chemicals used for pH adjustment and in chromatography analysis are HPLC analytical grade from Sigma Aldrich or Fluka. All aqueous solutions were prepared in deionized water obtained from Mill-Q™ system having  $18 \text{ m}\Omega \text{ cm}^{-1}$  resistivity.

### 2.2. Analytical methods

All the samples withdrawn at desired times, underwent a filtration through  $0.2 \mu\text{m}$  membrane filters before analysis. The pH was monitored using a pH-meter (Seven Compact S210, Mettler Toledo®). TOC and total nitrogen (TN) analysis was conducted using

**Table 1**  
Chemical formulas and structures of CLQ and its intermediates.

Substance	Chemical formula	Chemical structure
Chloroquine	C <sub>18</sub> H <sub>26</sub> ClN <sub>3</sub>	
7-chloro-4-quinolinamine	C <sub>9</sub> H <sub>7</sub> ClN <sub>2</sub>	
Oxamic acid	C <sub>2</sub> H <sub>3</sub> NO <sub>3</sub>	
Oxalic acid	C <sub>2</sub> H <sub>2</sub> O <sub>4</sub>	

Skalar Formacs<sup>HT</sup> TOC/TN analyzer. UV–Visible spectrophotometer (PerkinElmer Lambda 5) was used for rapid measurements of CLQ concentration at 278 nm using a 1 cm-quartz cells. H<sub>2</sub>O<sub>2</sub> concentration was evaluated by colorimetric method (at 420 nm) using titanium (IV) sulfate (Ti(SO<sub>4</sub>)<sub>2</sub>) for lower concentrations than 50 mg/L, while volumetric titration method with KMnO<sub>4</sub> was used for H<sub>2</sub>O<sub>2</sub> concentration > 50 mg/L (Eisenberg, 1943; Klassen et al., 1994). Active chlorine was measured by DPD colorimetric method using N,N-diethyl-*p*-phenylenediamine (Rice et al., 2017). Chlorides and nitrates were monitored using Dionex ICS 2000 ion chromatograph equipped with EGC eluent generator, Ion Pac AS 19 (4 mm × 250 mm) analytical separation column, ASRS 300 mm–4mm suppressor, and DS6 conductometric cell. Ammonium ions were analyzed by ion-selective electrode for ammonium ion (ELIT 8051 PVC membrane). CLQ and CQLA concentrations were measured by HPLC using Shimadzu 20A Gradient LC System with UV-VIS Detector equipped with Shim-pack GWS C18 (150×4.6, 5 μm) separation column. The separation was performed using a mobile phase composed of a mixture of eluent A (0.1% H<sub>3</sub>PO<sub>4</sub> in water) and eluent B (acetonitrile, CH<sub>3</sub>CN) in gradient elution mode at a fixed flow rate of 1 mL/min and constant column temperature at 40 °C. By injecting 10 μL of each sample, the gradient elution begun with 90% of eluent A during 5 min, then eluent A decreased to 40% within 15 min, and after that the elution gradient remains constant (40% A+60% B) until the end of analysis. The UV detector was set at a wavelength of 340 nm. Oxalic and oxamic acids were measured by HPLC using a Supelcogel H column (mobile phase, 0.15% phosphoric acid solution; flow rate, 0.15 mL/min) with UV detection at 210 nm. Linear calibration curves based on external standardization were obtained in chromatography analysis for all analytes with regression coefficients higher than 98%.

### 2.3. Experimental setup

A single-compartment glass electrochemical cell with a double jacket was used in all the electrochemical experiments. The temperature was maintained to 25 °C by water circulation. The cathode materials were made from carbon felt (Carbone Loraine, 15 × 4 × 0.5 cm<sup>3</sup>) and stainless steel in electro-Fenton oxidation and electrochemical oxidation, respectively. The anode materials used were BDD and platinum (Pt). Pt electrodes were obtained from Advent Research Materials (Oxford, England, UK). BDD anodes were

purchased from Adamant Technologies (Neuchatel, Switzerland). They were fabricated by hot filament chemical vapor deposition (HF CVD) technique of boron-doped diamond thin film deposited on single-crystal p-type Si (100) substrates (0.1 Ω cm Siltronix) as described elsewhere (Nasr et al., 2005). The cathode was attached to the wall of the electrochemical cell and the anode was placed in vertical position in the center 2 cm distant from the cathode. A fixed geometric area of 30 cm<sup>2</sup> for each electrode was immersed in the solution. The homogenization of the solutions was assured by continuous stirring using a magnetic stirrer (Thermo Scientific™ S8854105) at 300 rpm in all the experiments. The pH was adjusted to a desired value by adding aliquots of 0.1 M H<sub>2</sub>SO<sub>4</sub> or 0.1 M NaOH solutions. After pH adjustment and addition of an amount of the catalyst (FeSO<sub>4</sub>·7H<sub>2</sub>O) when needed, pure oxygen was continuously bubbled into 400 mL solution (0.05 M Na<sub>2</sub>SO<sub>4</sub>) nearby the cathode at a fixed flow rate in the range 60–240 mL/min. Electro-Fenton and anodic oxidation experiments were performed under galvanostatic mode (constant current density). The electrodes were connected to a digital dc power supply (Monacor PS-430) providing current and voltage in the ranges 0–30 A and 0–20 V. The current intensity applied during each experiment was maintained to a constant value using the power supply. A potentiometer (Micronal B474) was used to measure the cell voltage during the experiments. At certain time-periods, samples were withdrawn from the solution and then filtered by 0.45-mm membrane for analysis. During electrochemical oxidation experiments, BDD (or Pt) and stainless steel plates (effective area of 30 cm<sup>2</sup>) were inserted into the solution in parallel position and an inter-electrode gap of 2 cm.

## 3. Results and discussions

### 1. Generation of H<sub>2</sub>O<sub>2</sub> in electro-Fenton process

The generation of H<sub>2</sub>O<sub>2</sub> by electrochemical reduction of O<sub>2</sub> at the carbon felt cathode is main important stage in electro-Fenton process. The efficacy of this process depends largely on the rate of H<sub>2</sub>O<sub>2</sub> generation and the amount of H<sub>2</sub>O<sub>2</sub> available in solution to react with Fe<sup>2+</sup> ions and produce HO• radicals (Eqs (1) and (2)) (Brillas et al., 2009; Yu et al., 2015, 2014).

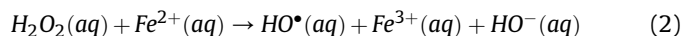
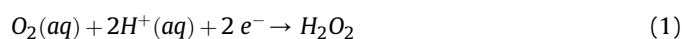
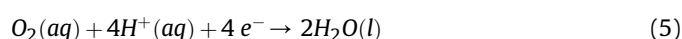
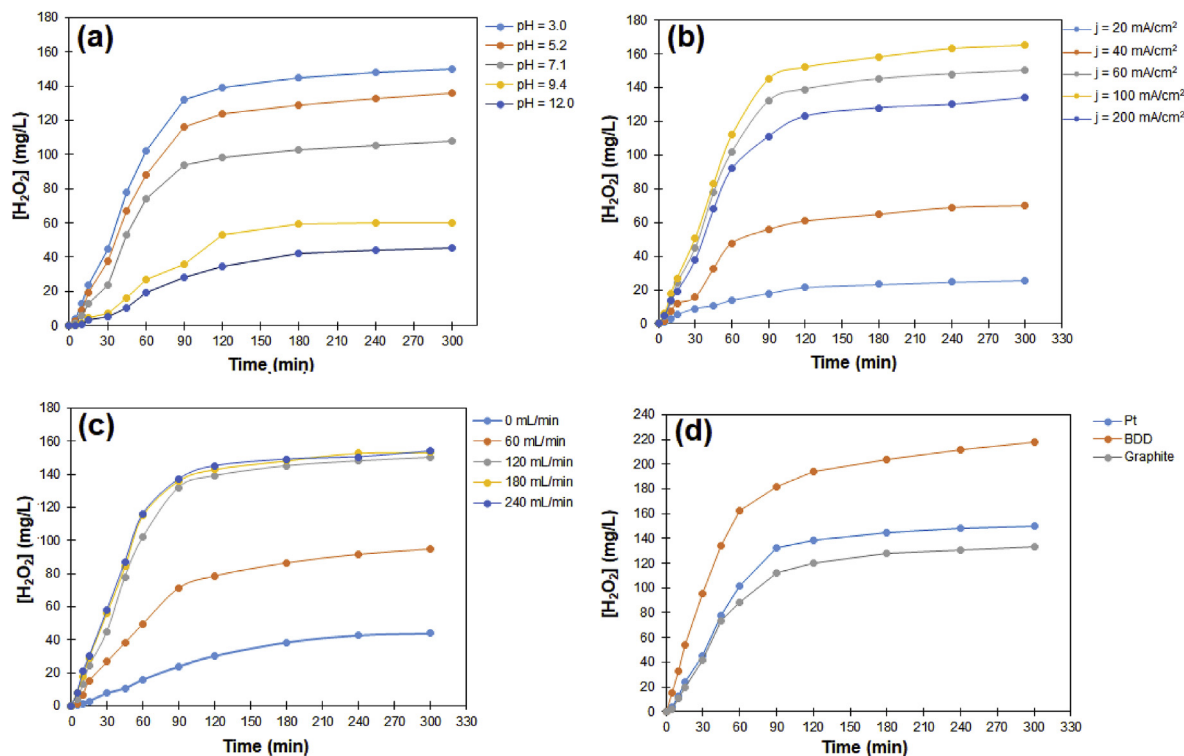


Fig. 1 presents the effects of pH, current density, O<sub>2</sub> flow rate, and anode material on the changes of H<sub>2</sub>O<sub>2</sub> concentration with time during the electrolysis of 0.05 M Na<sub>2</sub>SO<sub>4</sub> aqueous solutions. It is remarkable that the graphs of H<sub>2</sub>O<sub>2</sub> concentration via time have the same trend: A rapid linear increase in H<sub>2</sub>O<sub>2</sub> concentration from the beginning of the electrolysis to reach a maximum after 90–120 min, and then it is maintained to almost a constant value for a large plateau until the end (300 min). This result corresponds to steady state conditions at which the rate of generation of H<sub>2</sub>O<sub>2</sub> is equal to the rate of its destruction. This is probably due to the limited solubility of O<sub>2</sub>, mass/charge transfer kinetic limitations, and competition between the main reaction of generation of H<sub>2</sub>O<sub>2</sub> (Eq. (1)) and secondary reactions (Eqs. (3)–(6))





**Fig. 1.** Effects of (a) initial pH, (b) current density, (c) O<sub>2</sub> flow rate, and (d) anode material on the changes of H<sub>2</sub>O<sub>2</sub> concentration with time during electrolysis of 0.05 M Na<sub>2</sub>SO<sub>4</sub>. Experimental conditions: (a)  $j = 60 \text{ mA/cm}^2$ , O<sub>2</sub> flow rate = 80 mL/min, Anode: Pt (30 cm<sup>2</sup>), cathode: Carbon felt (30 cm<sup>2</sup>), T = 25 °C, stirring: 300 rpm; (b) pH = 3.0, O<sub>2</sub> flow rate = 80 mL/min, Anode: Pt (30 cm<sup>2</sup>), cathode: Carbon felt (30 cm<sup>2</sup>), T = 25 °C, stirring: 300 rpm; (c)  $j = 60 \text{ mA/cm}^2$ , pH = 3.0, Anode: Pt (30 cm<sup>2</sup>), cathode: Carbon felt (30 cm<sup>2</sup>), T = 25 °C, stirring: 300 rpm (d)  $j = 60 \text{ mA/cm}^2$ , pH = 3.0, O<sub>2</sub> flow rate = 80 mL/min, Anode: BDD/Pt/Graphite (30 cm<sup>2</sup>), cathode: Carbon felt (30 cm<sup>2</sup>), T = 25 °C, stirring: 300 rpm.



Fig. 1 a presents the effect of initial pH on the changes of H<sub>2</sub>O<sub>2</sub> concentration with time during electrolysis of 0.05 M Na<sub>2</sub>SO<sub>4</sub> using Carbon felt cathode and Pt anode at  $j = 60 \text{ mA/cm}^2$ , O<sub>2</sub> flow rate = 80 mL/min, T = 25 °C, and stirring at 300 rpm. As it can be seen from Fig. 1 a, the initial pH affected both the rate of H<sub>2</sub>O<sub>2</sub> generation and its maximum concentration. The average rate of H<sub>2</sub>O<sub>2</sub> generation decreased from 1.67 mg/min at pH 3.0 to 1.43, 1.13, 0.38, 0.27 mg/min at pH 5.2, 7.1, 9.4, and 12.0, respectively (the average rate was calculated from the slope of the linear ascending part of the graph). H<sub>2</sub>O<sub>2</sub> concentration decreased from 150 mg/L at pH 3.0 to 136, 108, 60.2, and 45.6 mg/L at pH 5.2, 7.1, 9.2, and 12.0, respectively (see Figure S1.a). The drop of the average rate of H<sub>2</sub>O<sub>2</sub> generation and its generated concentration at neutral and alkaline pH can be explained by the acceleration reactions of cathodic reduction and disproportionation of H<sub>2</sub>O<sub>2</sub> at neutral and alkaline conditions (Eqs. (3) and (7)) (Shemer and Linden, 2006; Teymori et al., 2020). A value of pH around 3.0 is optimal for H<sub>2</sub>O<sub>2</sub> generation by electrochemical reduction of O<sub>2</sub> at carbon-felt cathode.

Fig. 1 b presents the effect of current density on the changes of H<sub>2</sub>O<sub>2</sub> concentration with time during electrolysis of 0.05 M Na<sub>2</sub>SO<sub>4</sub> using Carbon felt cathode and Pt anode at pH = 3.0, O<sub>2</sub> flow rate = 80 mL/min, T = 25 C, stirring at 300 rpm. Fig. 1 b demonstrates that the increase of current density from 20 to 100 mA/cm<sup>2</sup> enhanced the generation of H<sub>2</sub>O<sub>2</sub>; however, at 200 mA/cm<sup>2</sup> a decrease in H<sub>2</sub>O<sub>2</sub> generation was observed. The accumulated H<sub>2</sub>O<sub>2</sub> concentration passed from 25.8 mg/L at 20 mA/cm<sup>2</sup> to 70.1, 150, 165, and 136 mg/L at 40, 60, 100, and 200 mA/cm<sup>2</sup>, respectively. The

average rates of H<sub>2</sub>O<sub>2</sub> generation were 0.25, 0.74, 1.67, 1.83, and 1.48 at current densities of 20, 40, 60, 100, and 200 mA/cm<sup>2</sup>, respectively (see Figure S1.b). It seems that at higher current density than 60 mA/cm<sup>2</sup>, the electrochemical reduction of O<sub>2</sub> to H<sub>2</sub>O (Eq. (5)) starts to compete with the main reaction of H<sub>2</sub>O<sub>2</sub> generation (Eq. (1)). In addition, at high current density, the electro-generated H<sub>2</sub>O<sub>2</sub> can be oxidized at the anode (Eq. (8)).



Fangke et al. (Yu et al., 2014) reported similar results related to the effect of current density on H<sub>2</sub>O<sub>2</sub> generation during electrolysis using graphite felt cathode. Several studies (Y. Gao et al., 2020; Özcan et al., 2008; Wang et al., 2019; Zhou et al., 2013) correlated the decrease of H<sub>2</sub>O<sub>2</sub> generation at high current density with the decrease in the cathode potential with the increase of current density, which results in greater competition between the reduction of oxygen to H<sub>2</sub>O<sub>2</sub> and to H<sub>2</sub>O (Eqs. (1) and (5)). A current density of 60 mA/cm<sup>2</sup> is cost-effective to generate H<sub>2</sub>O<sub>2</sub> from the reduction of O<sub>2</sub> at carbon-felt cathode.

Fig. 1 c presents the effect of O<sub>2</sub> flow rate on the changes of H<sub>2</sub>O<sub>2</sub> concentration with time during electrolysis of 0.05 M Na<sub>2</sub>SO<sub>4</sub> using Carbon felt cathode and Pt anode at  $j = 60 \text{ mA/cm}^2$ , pH = 3.0, T = 25 °C, and stirring at 300 rpm. It is noticeably observed that H<sub>2</sub>O<sub>2</sub> can be generated even without bubbling O<sub>2</sub> in the solution (O<sub>2</sub> flow rate = 0 mL/min) with a low average rate of 0.24 mg/L and its accumulated concentration reached 43.8 mg/L. This generation of H<sub>2</sub>O<sub>2</sub> in absence of O<sub>2</sub> bubbling resulted from the electrochemical reduction of the dissolved O<sub>2</sub> from air and the additional O<sub>2</sub> electro-generated at the anode from water discharge (Y. Gao et al., 2020; Özcan et al., 2008; Wang et al., 2019; Zhou et al., 2013). The increase of O<sub>2</sub> flow rate from 40 mL/min to 80 mL/min increased the average



rate of H<sub>2</sub>O<sub>2</sub> generation and the accumulated H<sub>2</sub>O<sub>2</sub> concentration from 0.84 mg/min and 94.9 mg/L to 1.67 mg/min and 150 mg/L, respectively (see Figure S1.c). Further increase in O<sub>2</sub> flow rate does not have a significant effect on H<sub>2</sub>O<sub>2</sub> generation. Bubbling O<sub>2</sub> in a solution increases the concentration of O<sub>2</sub> in water. In addition, the increase in the O<sub>2</sub> flow rate improves the mass transfer kinetics. When the solution is saturated in O<sub>2</sub> (saturated solution contains 8.3 mg O<sub>2</sub>/L at 1.0 atm and 25 °C), the increase of O<sub>2</sub> flow rate (>80 mL/min) will not affect the accumulated H<sub>2</sub>O<sub>2</sub> concentration. A flow rate of 80 mL/min of pure oxygen is adequate to produce high-accumulated H<sub>2</sub>O<sub>2</sub> concentration.

Fig. 1 d presents the changes of H<sub>2</sub>O<sub>2</sub> concentration with time during electrolysis of 0.05 M Na<sub>2</sub>SO<sub>4</sub> using Carbon felt cathode and different anode materials (Pt, BDD, graphite) at *j* = 60 mA/cm<sup>2</sup>, pH = 3.0, O<sub>2</sub> flow rate = 80 mL/min, T = 25 °C, and stirring at 300 rpm. The average rates of H<sub>2</sub>O<sub>2</sub> generation were 2.75, 1.67 and 1.49 mg/min for BDD, Pt, and graphite anodes, respectively. The accumulated H<sub>2</sub>O<sub>2</sub> concentrations measured at the end of electrolysis were 218, 150, and 133 mg/L for BDD, Pt, and graphite anodes, respectively (see Figure S1.d). BDD anode showed better H<sub>2</sub>O<sub>2</sub> generation compared with Pt and graphite anode materials. This result can be explained by the large voltage window and the high over potential of O<sub>2</sub> evolution of BDD anode (Marselli et al., 2003; Michaud et al., 2003). BDD anode, in fact, can produce large amounts of hydroxyl radicals from water oxidation that combine together to form H<sub>2</sub>O<sub>2</sub> (Eqs. (9) and (10)) (Marselli et al., 2003; Michaud et al., 2003). Similar results were reported in the literature confirming higher performance of BDD anode in electro-Fenton oxidation (Borràs et al., 2013; El-Ghenymy et al., 2015; Pereira et al., 2016; Ruiz et al., 2011).



Pairing carbon felt cathode with BDD anode generates additional amount of H<sub>2</sub>O<sub>2</sub> compared to the other configurations. Accordingly, the combination of anodic oxidation using BDD and the electrogeneration of H<sub>2</sub>O<sub>2</sub> by reduction of O<sub>2</sub> at carbon felt electrode would result in high efficacy to electro-Fenton oxidation of organic pollutants.

## 2. Efficiency of electro-Fenton oxidation in the degradation of CLQ

Fig. 2 presents the changes of CLQ concentration with time during the electrochemical treatment of 125 mg/L CLQ aqueous solutions by anodic oxidation using Pt (Electrolysis-Pt) and BDD (Electrolysis-BDD) anodes and stainless steel cathode and by electro-Fenton oxidation (O<sub>2</sub> flow rate = 80 mL/min; Fe<sup>2+</sup>: 10 mg/L) using carbon felt cathode and Pt (Electro-Fenton-Pt) and BDD (Electro-Fenton-BDD) anodes holding the other experimental conditions unvaried (0.05 M Na<sub>2</sub>SO<sub>4</sub>, *j* = 60 mA/cm<sup>2</sup>, pH = 3.0, T = 25 °C, stirring at 300 rpm). CLQ concentration decreased with time in all the experiments, but at different extent. The efficiency of CLQ degradation (in terms of kinetics and % of CLQ depletion) is increasing in the order: Electrolysis-Pt < Electrolysis-BDD < Electro-Fenton-Pt < Electro-Fenton-BDD. Assuming pseudo-first order kinetics for CLQ degradation (exponential decay of CLQ concentration), the rate constants, *k*<sub>obs</sub> calculated for a pseudo-first order degradation, were 0.001, 0.006, 0.011, and 0.029 min<sup>-1</sup> for electrolysis-Pt, electrolysis-BDD, electro-Fenton-Pt, and electro-Fenton-BDD, respectively. Electro-Fenton-BDD achieved the complete depletion CLQ after 180 min; however, 84%, 68%, and 17% of CLQ were removed during the same period of time (180 min), electro-Fenton-Pt, electrolysis-BDD, and electrolysis-Pt,

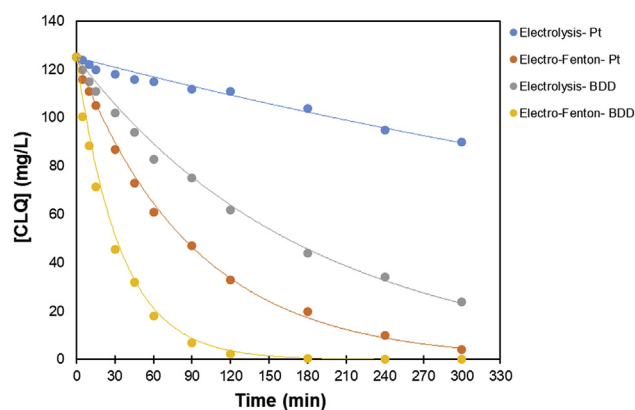


Fig. 2. Changes of CLQ concentration with time during electrochemical treatment of 125 mg/L CLQ aqueous solutions by anodic oxidation and electro-Fenton oxidation. Experimental conditions: Electrolyte: 0.05 M Na<sub>2</sub>SO<sub>4</sub>, *j* = 60 mA/cm<sup>2</sup>, pH = 3.0, T = 25 °C, stirring = 300 rpm; Electrolysis-Pt: Anode: Pt, Cathode: Stainless steel; Electrolysis-BDD: Anode: BDD, Cathode: Stainless steel; Electro-Fenton-Pt: Anode Pt, Cathode: Carbon felt, O<sub>2</sub> flow rate: 80 mL/min, Fe<sup>2+</sup>: 10 mg/L; Electro-Fenton-BDD: Anode: BDD, Cathode: Carbon felt, O<sub>2</sub> flow rate: 80 mL/min, Fe<sup>2+</sup>: 10 mg/L.

respectively. The anode material has a significant influence on CLQ degradation in both anodic oxidation and electro-Fenton.

This can be explained by the larger electrochemical activity of BDD than Pt anode in 0.05 M Na<sub>2</sub>SO<sub>4</sub> enabling the direct oxidation of organic molecules on the surface of BDD anode (Martínez-Huitle and Panizza, 2018; Panizza et al., 2008). BDD anode can produce large amounts of hydroxyl radicals (HO<sup>•</sup>) from the electrochemical oxidation of water (Eq. (9)), which are weakly adsorbed on BDD surface resulting in immediate and non-selective reactions with the organic pollutant molecules (Marselli et al., 2003; Michaud et al., 2003). Furthermore, the electrochemical oxidation of sulfate ions at BDD anode yields the formation of strong oxidants (sulfate radicals, SO<sub>4</sub><sup>•-</sup> and persulfate ions, S<sub>2</sub>O<sub>8</sub><sup>2-</sup>) as shown by the following reactions (Eqs. (11) and (12)) (Michaud et al., 2000; Serrano et al., 2002):



These oxidants participate in the degradation of organic pollutants in solution. Furthermore, Michaud et al. (2003) stated that O<sub>3</sub> and H<sub>2</sub>O<sub>2</sub> could also be produced by anodic oxidation of water at high current density.

In addition, the results demonstrate higher efficiency of electro-Fenton oxidation compared to anodic oxidation (for Pt and BDD anodes) in degrading CLQ. This is probably due to larger production of hydroxyl radicals from catalytic decomposition of the electro-generated H<sub>2</sub>O<sub>2</sub> by Fe<sup>2+</sup> in solution. In the case of BDD, anodic oxidation of water at the anode produces supplementary hydroxyl radicals, which clarifies the better performance of electro-Fenton with BDD anode than with Pt anode.

The highest efficiency of electro-Fenton oxidation using BDD anode compared to the other electrochemical methods can be explained by the contribution of different pathways in CLQ degradation including (i) the mediated oxidation by hydroxyl radicals produced by Fenton reaction between H<sub>2</sub>O<sub>2</sub> electrogenerated at carbon felt cathode and Fe<sup>2+</sup> ions in solution, (ii) the indirect oxidation via hydroxyl and sulfate radicals electrogenerated at the BDD anode from water oxidation locally close to BDD surface; (iii) the indirect oxidation via sulfate radicals electrogenerated from direct oxidation of sulfate ions at BDD surface and/or by the

reaction of sulfate ions with HO<sup>•</sup> radicals produced at BDD surface from water discharge at BDD surface (de Freitas Araújo et al., 2020; Escalona-Durán et al., 2020); (iv) mediated chemical oxidation in solution by the inorganic strong oxidants (persulfate ions, O<sub>3</sub>, H<sub>2</sub>O<sub>2</sub>) produced by anodic and cathodic reactions involving the electrolyte, (v) direct electrochemical oxidation of CLQ at the surface of BDD anode.

### 3. Effects of operating conditions on electro-Fenton oxidation of CLQ

Fig. 3 presents the changes of the normalized concentration ( $[\text{CLQ}]_t/[\text{CLQ}]_0$ ) with time ( $[\text{CLQ}]_0$  is the initial CLQ concentration at  $t = 0$  s,  $[\text{CLQ}]_t$  is CLQ concentration at an instant  $t$ ) during electro-Fenton oxidation of 0.05 M Na<sub>2</sub>SO<sub>4</sub> aqueous solutions containing different CLQ concentrations using carbon felt cathode and BDD anode keeping the other operating conditions fixed ( $j = 60$  mA/cm<sup>2</sup>, pH = 3.0, O<sub>2</sub> flow rate = 80 mL/min, [Fe<sup>2+</sup>] = 10 mg/L, T = 25 °C, stirring = 300 rpm). As it can be seen, the normalized CLQ concentration decreased exponentially with time for all the initial concentrations studied indicating a pseudo-first order kinetics for CLQ degradation by electro-Fenton-BDD oxidation. It is important to report that CLQ was completely depleted by electro-Fenton-BDD oxidation in regardless of CLQ concentration (for  $[\text{CLQ}] \leq 250$  mg/L). The increase of initial concentration increased the time required to deplete CLQ from water: 90 min for  $[\text{CLQ}] = 34$  mg/L, 120 min for  $[\text{CLQ}] = 75$  mg/L, 180 min for  $[\text{CLQ}] = 125$  mg/L, 240 min for  $[\text{CLQ}] = 200$ , and 300 min for  $[\text{CLQ}] = 250$  mg/L. Moreover, the inlet graph of Fig. 3 shows that the pseudo-first order rate constant  $k_{\text{obs}}$  decreased with the increase of CLQ concentration for  $[\text{CLQ}] < 200$  mg/L, and then it remained almost constant  $[\text{CLQ}] \geq 200$  mg/L. This results indicates that, for  $[\text{CLQ}] < 200$  mg/L, the reaction is not truly first order reaction (although good first order fitting was observed for each concentration). For  $[\text{CLQ}] < 200$  mg/L, the generated amount of hydroxyl radicals is high enough and it stays unchanged during the electro-Fenton-BDD oxidation, which does not affect the kinetics of CLQ degradation; while for  $[\text{CLQ}] \geq 200$  mg/L, the amount of hydroxyl radicals becomes the critical parameter that determines CLQ degradation kinetics.

Fig. 4 a presents the effect of pH on the changes of CLQ concentration with time during electro-Fenton oxidation of 125 mg/L CLQ aqueous solutions using carbon felt cathode and BDD anode

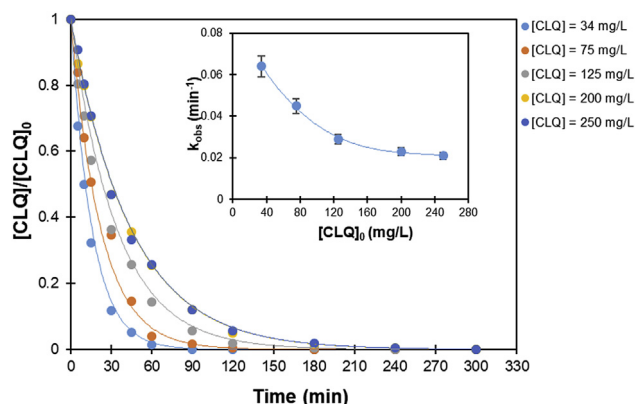


Fig. 3. Changes of normalized concentration ( $[\text{CLQ}]_t/[\text{CLQ}]_0$ ) with time ( $[\text{CLQ}]_0$ ) during electro-Fenton oxidation of 0.05 M Na<sub>2</sub>SO<sub>4</sub> aqueous solutions containing different CLQ concentrations using carbon felt cathode and BDD anode. Inlet graph: the changes of pseudo-first order rate constant  $k_{\text{obs}}$  versus CLQ concentration. Experimental conditions:  $j = 60$  mA/cm<sup>2</sup>, pH = 3.0, O<sub>2</sub> flow rate = 80 mL/min, [Fe<sup>2+</sup>] = 10 mg/L, T = 25 °C, stirring = 300 rpm.

holding the other operating parameters fixed (Electrolyte: 0.05 M Na<sub>2</sub>SO<sub>4</sub>,  $j = 60$  mA/cm<sup>2</sup>, O<sub>2</sub> flow rate = 80 mL/min, [Fe<sup>2+</sup>] = 10 mg/L, T = 25 °C, stirring = 300 rpm). The profile of CLQ concentration with time exhibited an exponential decrease with time for all the pH values in the range 3.0–12.0. The complete depletion was achieved for pH = 3.0 after 180, while the percentages of CLQ depletion after the same period of time were 93, 81, 54, 29% at pH values 5.2, 7.1, 9.4, and 12.0, respectively. The rate of CLQ depletion decreased with the increase of pH value from 3.0 to 12.0 as shown in Fig. 4 b. These results are in good correlation with the results presented in Fig. 1 a, where it was shown that the highest H<sub>2</sub>O<sub>2</sub> generation occurred at pH = 3.0. The higher efficiency of electro-Fenton oxidation in depleting CLQ at pH = 3.0 is due to larger production of hydroxyl radicals from catalytic decomposition of H<sub>2</sub>O<sub>2</sub> by Fe<sup>2+</sup>.

Fig. 5 presents the effect of current density on the changes of CLQ concentration with time during electro-Fenton oxidation of 125 mg/L CLQ aqueous solutions using carbon felt cathode and BDD anode holding the other operating parameters fixed (Electrolyte: 0.05 M Na<sub>2</sub>SO<sub>4</sub>, pH = 3.0, O<sub>2</sub> flow rate = 80 mL/min, [Fe<sup>2+</sup>] = 10 mg/L, T = 25 °C, stirring = 300 rpm). The complete depletion of CLQ was accomplished after 120 min at 200 mA/cm<sup>2</sup>. After 120 min of the starting of electro-Fenton experiments, the % of CLQ depletion was 49.6, 72.8, 98.1, and 98.6 at 20, 40, 60, and 100 mA/cm<sup>2</sup>, respectively. Fitting the data to pseudo-first order kinetics showed that the rate constant  $k_{\text{obs}}$  increased linearly with current density between 20 and 100 mA/cm<sup>2</sup>, then it became almost unvaried with the increase of the current density (see inlet graph in Fig. 5).

The specific electric charge consumption calculated from the following formula:

$$Q \left( \frac{A \cdot h}{g \text{ HCQ}} \right) = \frac{j \left( \frac{\text{mA}}{\text{cm}^2} \right) \times A (\text{cm}^2) \times t (\text{s})}{3600 \left( \frac{\text{s}}{\text{h}} \right) \times V (\text{L}) \times [\text{CLQ}] \left( \frac{\text{mg}}{\text{L}} \right)}$$

where  $j$  is the current density,  $A$  is the electrode area,  $t$  is the time required for complete depletion,  $V$  the volume of the reactor, and  $[\text{CLQ}]$  is CLQ concentration. The estimated values of  $Q$  are illustrated in Table 2. The results showed that similar specific electrical charge consumption are required during the electro-Fenton oxidation at current density  $\leq 60$  mA/cm<sup>2</sup>. Increasing the current density to values higher than 60 mA/cm<sup>2</sup>, increases significantly the specific electrical charge consumption.

It can be concluded that the increase of current from 20 to 60 mA/cm<sup>2</sup> enhanced the kinetics and efficiency of electro-Fenton oxidation of CLQ; however, higher current density than 60 mA/cm<sup>2</sup> showed minor improvement and higher specific electric charge consumption. Increasing the current density up to 60 mA/cm<sup>2</sup> (i) enhances the generation of H<sub>2</sub>O<sub>2</sub> from electrochemical reduction of O<sub>2</sub> at the cathode (Fig. 1b) producing larger amounts of HO<sup>•</sup> radicals by catalytic decomposition with Fe<sup>2+</sup> in solution, (ii) generates substantial HO<sup>•</sup> radicals from the discharge of water at BDD anode, (iii) produces strong oxidants from the anodic oxidation of sulfate at BDD anode (sulfate radicals and persulfate ions) that participate in the degradation of CLQ and its intermediates, (iv) accelerates the direct anodic oxidation of CLQ and its intermediates on the surface of BDD electrode. However, higher current densities than 60 mA/cm<sup>2</sup> accelerates the secondary reactions of H<sub>2</sub>O<sub>2</sub> disproportionation in solution, H<sub>2</sub> evolution at the cathode and O<sub>2</sub> evolution at the anode, and makes them highly competitive with the primary reactions of generation of H<sub>2</sub>O<sub>2</sub> at the cathode and HO<sup>•</sup> radicals at the anode. This results in generating similar amount of HO<sup>•</sup> radicals to attack the same organic pollution than at 60 mA/cm<sup>2</sup>, which rises the electrical energy requirements, and then augments the overall

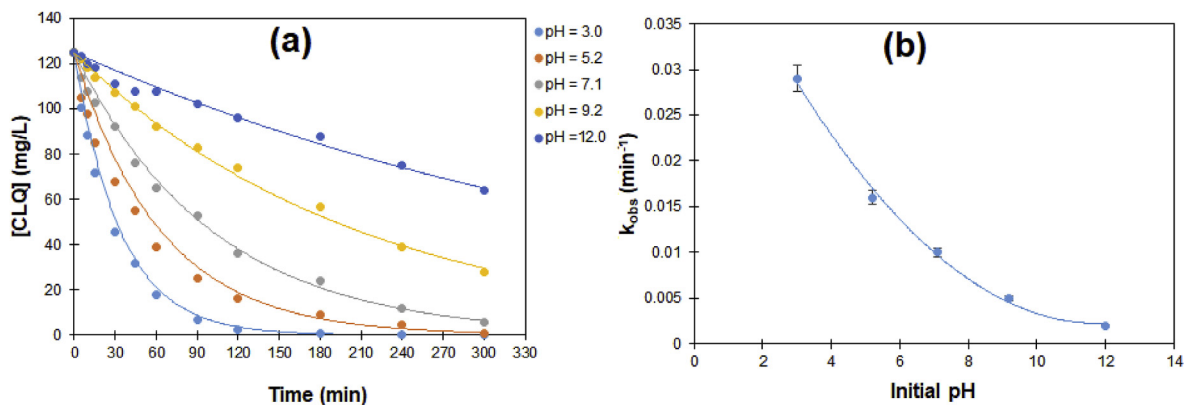


**Fig. 4.** Changes of: (a) CLQ concentration with time at different pH values during electro-Fenton oxidation of 125 mg/L CLQ aqueous solutions using carbon felt cathode and BDD anode, and (b) pseudo-first order rate constant  $k_{obs}$  versus initial pH. Experimental conditions: Electrolyte: 0.05 M  $\text{Na}_2\text{SO}_4$ ,  $j = 60 \text{ mA/cm}^2$ ,  $\text{O}_2$  flow rate = 80 mL/min,  $[\text{Fe}^{2+}] = 10 \text{ mg/L}$ ,  $T = 25 \text{ }^\circ\text{C}$ , stirring = 300 rpm.

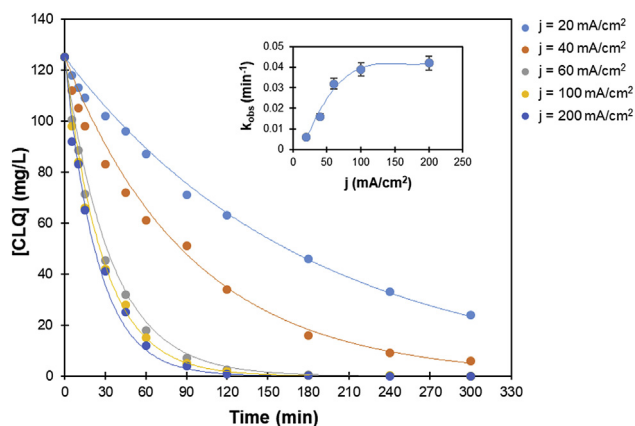


**Fig. 5.** Changes of CLQ concentration with time at different current densities (20–200  $\text{mA/cm}^2$ ) during electro-Fenton oxidation of 125 mg/L CLQ aqueous solutions using carbon felt cathode and BDD anode. Inlet: pseudo-first order rate constant  $k_{obs}$  versus current density. Experimental conditions: Electrolyte: 0.05 M  $\text{Na}_2\text{SO}_4$ ,  $\text{pH} = 3.0$ ,  $\text{O}_2$  flow rate = 80 mL/min,  $[\text{Fe}^{2+}] = 10 \text{ mg/L}$ ,  $T = 25 \text{ }^\circ\text{C}$ , stirring = 300 rpm.

**Table 2**

Estimated specific electric charge consumption during electro-Fenton oxidation of 125 mg/L CLQ aqueous solutions using carbon felt cathode and BDD anode at different current densities (same experimental conditions than Fig. 2).

Current density ( $\text{mA/cm}^2$ )	Time required for complete CLQ depletion (min)	Q (Ah/g HCO)
20	320	129.0
40	240	131.9
60	210	128.5
100	150	152.2
200	120	241.7

costs of the electro-Fenton oxidation.

Fig. 6 a presents the effect of  $\text{Fe}^{2+}$  dose on the changes of CLQ concentration during with time during the first 60 min of electro-Fenton oxidation of 125 mg/L CLQ aqueous solutions using carbon felt cathode and BDD and Pt anodes using the same operating parameters (Electrolyte: 0.05 M  $\text{Na}_2\text{SO}_4$ ,  $j = 60 \text{ mA/cm}^2$ ,  $\text{pH} = 3.0$ ,  $\text{O}_2$  flow rate = 80 mL/min,  $T = 25 \text{ }^\circ\text{C}$ , stirring = 300 rpm). The degradation of CLQ occurred even in absence of  $\text{Fe}^{2+}$  and 8% and 51% of CLQ were removed by electro-Fenton-Pt and electro-Fenton-BDD after 60 min. This can be explained by the contribution of  $\text{HO}^\bullet$  radicals produced at the anode surface in the degradation of CLQ. The addition of  $\text{Fe}^{2+}$  enhanced the efficiency of CLQ degradation for

both electro-Fenton-Pt and electro-Fenton-BDD; however, the highest % CLQ depletion by electro-Fenton-Pt did not exceed that obtained by electro-Fenton-BDD in absence of  $\text{Fe}^{2+}$ . This result confirms the important contribution of anodic oxidation using BDD on the overall efficiency of electro-Fenton oxidation (Borrás et al., 2013; El-Ghenymy et al., 2015; Pereira et al., 2016; Ruiz et al., 2011).

The increase of  $\text{Fe}^{2+}$  dose increased the % CLQ depletion for both electro-Fenton-Pt and electro-Fenton-BDD. After 60 min electro-Fenton-Pt oxidation, the % CLQ depletion increased from 8% in absence of  $\text{Fe}^{2+}$  to 26.4, 33.6, and 37.6 in presence of 5, 10, and 20 mg  $\text{Fe/L}$ , respectively. For the same period of time electro-Fenton-BDD achieved 51% in absence of  $\text{Fe}^{2+}$  and 75.2, 85.6, and 92.8 in presence of 5, 10, and 20 mg  $\text{Fe/L}$ , respectively. The enhancement of % CLQ depletion by increasing  $\text{Fe}^{2+}$  dose is mainly due to the acceleration of Fenton reaction ( $\text{H}_2\text{O}_2$  decomposition into  $\text{HO}^\bullet$  radicals by  $\text{Fe}^{2+}$ ) and the rapid regeneration of  $\text{Fe}^{2+}$  catalyst by the electrochemical reduction of  $\text{Fe}^{3+}$  at carbon felt cathode. The rate constant  $k_{obs}$  obtained from fitted data to pseudo-first order kinetics increases with the increase of  $\text{Fe}^{2+}$  dose. This increase is more important for electro-Fenton-BDD as shown in

Fig. 6 b. However, higher  $\text{Fe}^{2+}$  doses than 10 mg  $\text{Fe/L}$  had less impact on the kinetics and efficiency of electro-Fenton, which can be due to partial precipitation of  $\text{Fe}^{3+}$  as  $\text{Fe}(\text{OH})_3$  and formation Fe-oxalate complexes decelerating the regeneration of  $\text{Fe}^{2+}$  catalyst.

#### 4. Intermediates of CLQ degradation by electro-Fenton oxidation

Fig. 7 a presents the changes of the concentrations (in mg C/L) of CLQ, TOC, and intermediates (calculated from mass balance) during the electro-Fenton oxidation of 125 mg/L CLQ aqueous solutions using carbon felt cathode and BDD and Pt anodes using under the optimized operating conditions (Electrolyte: 0.05 M  $\text{Na}_2\text{SO}_4$ ,

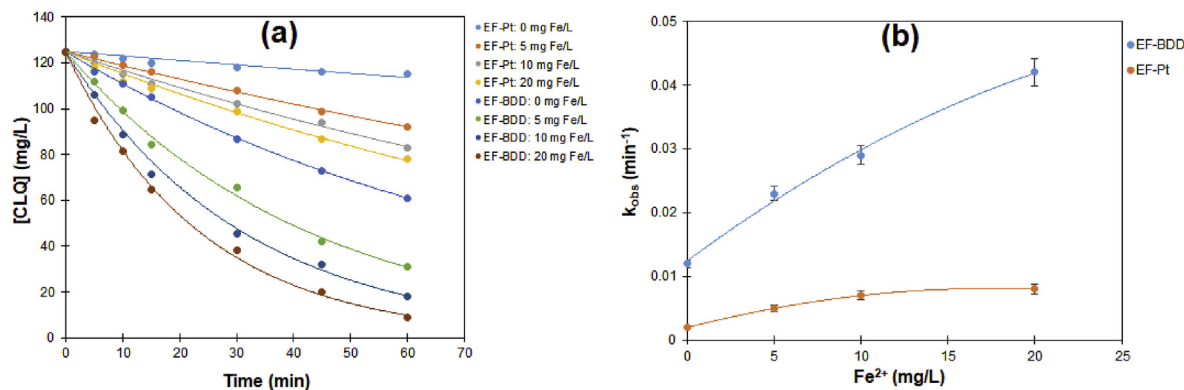


**Fig. 6.** Changes of: (a) CLQ concentration with time at different Fe<sup>2+</sup> doses during electro-Fenton oxidation of 125 mg/L CLQ aqueous solutions using carbon felt cathode and BDD anode, and (b) pseudo-first order rate constant  $k_{obs}$  versus Fe<sup>2+</sup> dose. Experimental conditions: Electrolyte: 0.05 M Na<sub>2</sub>SO<sub>4</sub>,  $j = 60$  mA/cm<sup>2</sup>, pH = 3.0, O<sub>2</sub> flow rate = 80 mL/min, T = 25 °C, stirring = 300 rpm.

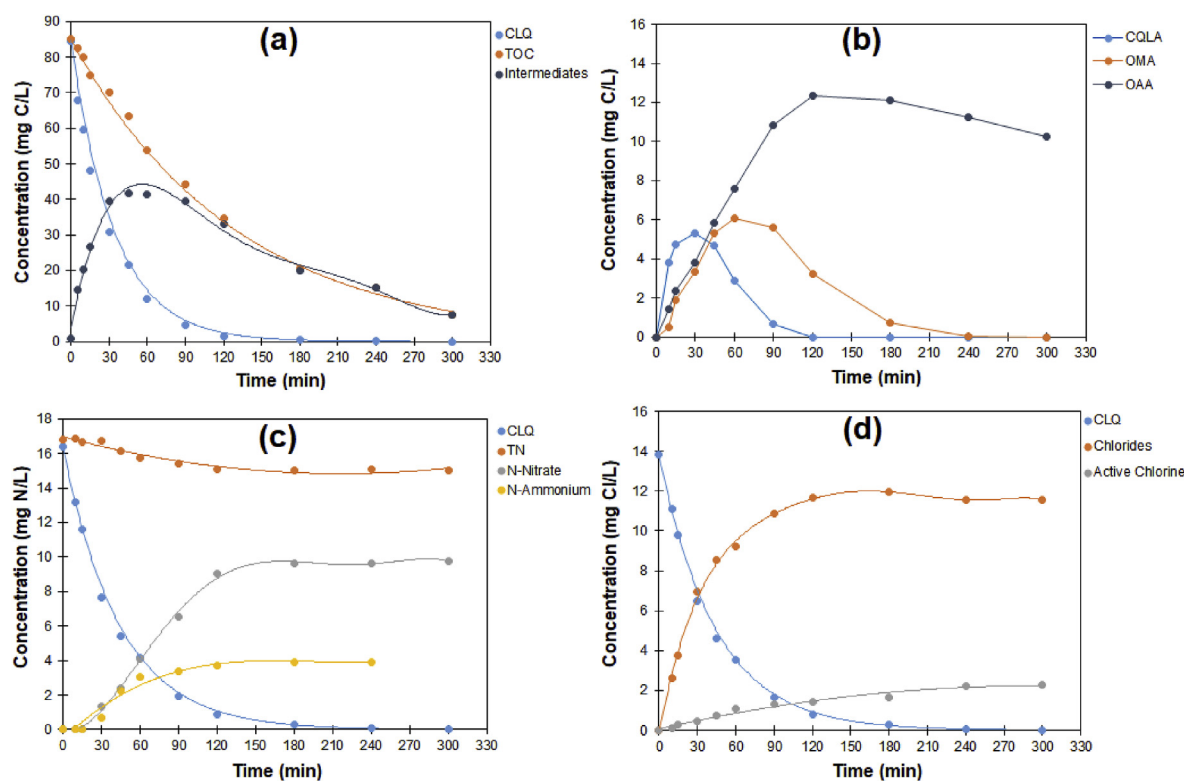


**Fig. 7.** Changes with time of: (a) TOC and intermediates, (b) Chlorides and active chlorine, (c) Nitrogen intermediates, (d) organic intermediates during electro-Fenton oxidation of 125 mg/L CLQ aqueous solutions using carbon felt cathode and BDD anode. Experimental conditions: Electrolyte: 0.05 M Na<sub>2</sub>SO<sub>4</sub>,  $j = 60$  mA/cm<sup>2</sup>, pH = 3.0, O<sub>2</sub> flow rate = 80 mL/min, Fe<sup>2+</sup> = 10 mg/L, T = 25 °C, stirring = 300 rpm.

$j = 60$  mA/cm<sup>2</sup>, pH = 3.0, O<sub>2</sub> flow rate = 80 mL/min, Fe<sup>2+</sup> = 10 mg/L, T = 25 °C, stirring = 300 rpm). CLQ and TOC concentrations decreased continuously with time with different rates, while the intermediates concentration increased from the beginning of the treatment to reach a maximum after 60 min, and then decreased with the same profile than TOC. The continuous decrease of TOC indicates that the organic carbon is transformed into CO<sub>2</sub> from the beginning electro-Fenton-BDD. Assuming pseudo-first order kinetics for CLQ and TOC, the rate constant determined by fitting was 0.029 and 0.008 min<sup>-1</sup> for CLQ and TOC, respectively. This results confirms the formation of organic intermediates at the first stages of CLQ the degradation by electro-Fenton oxidation. The overlapping of the profiles of TOC and the intermediates demonstrates

the persistence of certain organic intermediates until the end of the treatment (300 min), where 92% TOC was eliminated.

The results of HPLC analysis for CQLA (7-chloro-4-quinolinamine), OMA (oxamic acid), and OAA (oxalic acid) expected as intermediates of degradation are given in Fig. 7 b. The profiles of CQLA and OMA concentrations are similar with a rapid increase to reach maxima of 5.3 and 6.1 mg C/L at 30 and 60 min, and then they rapidly decreased to disappear after 120 and 240 min, respectively. OAA exhibited a slow accumulation to reach a maximum concentration of 12.3 mg C/L after 120 min, and then underwent a sluggish decrease to persist at 7.4 mg C/L at the end of the treatment. These results endorse the formation of aromatic intermediates including CQLA at the first stages of the electro-



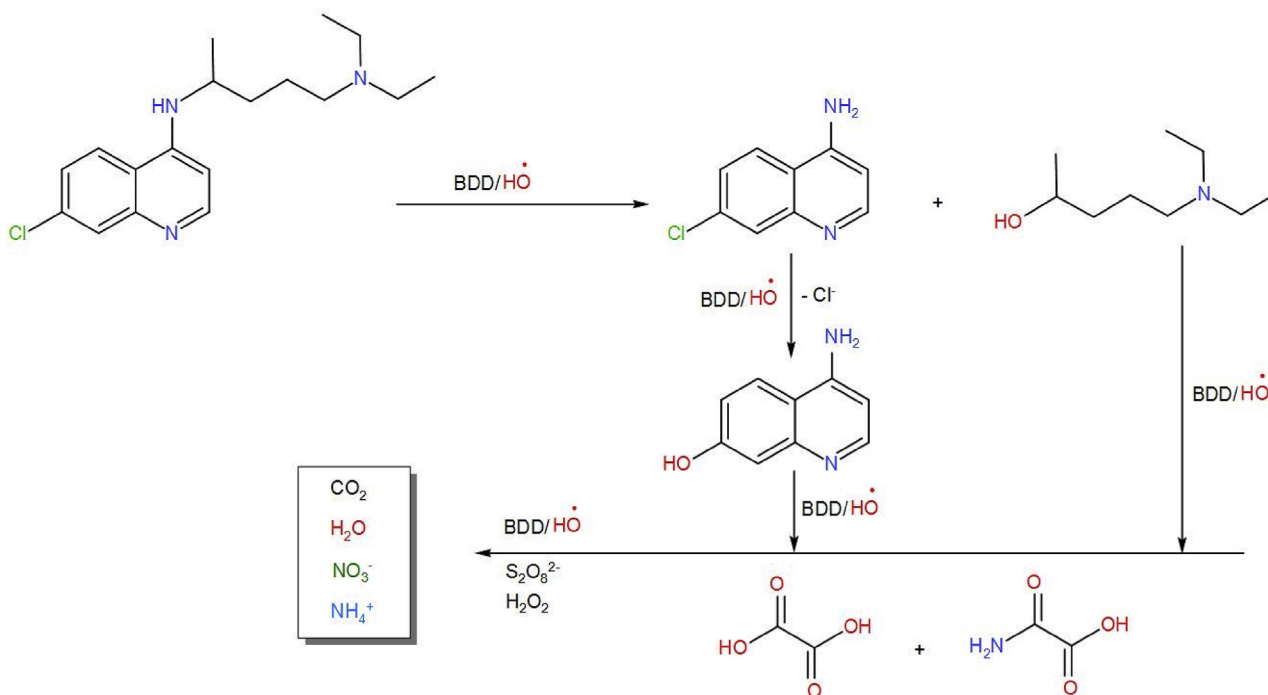


Fig. 8. Simple mechanism for CLQ degradation by electro-Fenton oxidation.

Fenton oxidation of CLQ. These intermediates undergo a rapid oxidative of the aromatic rings into aliphatic intermediates including carboxylic acids (OMA and OAA). The latter are slowly degraded and take long time to be mineralized due to the formation of stable complexes with Fe<sup>2+</sup>/Fe<sup>3+</sup> that resist to HO• radicals attack as mentioned in literature by several authors (El-Ghenymy et al., 2015; Garcia-Segura and Brillas, 2011; Gong et al., 2016). The mineralization of the target compound was confirmed by the release of inorganic nitrogen ions and chlorides as shown Fig. 7c and 8d. The organic nitrogen was mainly released in the form of nitrates, NO<sub>3</sub><sup>-</sup> and ammonium ions, NH<sub>4</sub><sup>+</sup> as shown in Fig. 7c. Nitrates and ammonium ions started to form after 30 min of the starting of the electrolysis indicating that the release of nitrogen does not happen at the first stages of CLQ degradation by electro-Fenton oxidation. After that, NO<sub>3</sub><sup>-</sup> and NH<sub>4</sub><sup>+</sup> concentrations raised to reach plateaus after 120 min at 9.7 and 4.0 mg N/L, respectively. The total nitrogen (TN) declined a little bit from 16.8 to 15.0 mg N/L at the end of electrolysis indicating that a small part of organic nitrogen was volatilized in the form of NH<sub>3</sub>, NO<sub>x</sub>, and chloramines (Dbira et al., 2015; Zöllig et al., 2015). In contrast, chlorides were released from the beginning of the treatment as shown in the changes of the concentration of chlorides presented in Fig. 7d. Chlorides concentration increased rapidly to reach a maximum value of 12.0 mg Cl/L (84% of total chlorine) after 120 min, then it remained stable until the end of the treatment. A small amount of active chlorine (HClO and ClO<sup>-</sup>) was measured during the treatment with a maximum of 2.3 mg Cl/L (16% of total chlorine). Active chlorine is formed by reaction of HO• radicals with chlorides in solution or at immediate vicinity of BDD surface (Martínez-Huitle and Panizza, 2018). Based on these results a simple mechanism for CLQ degradation by electro-Fenton oxidation is proposed in Fig. 8. CLQ degradation starts by dealkylation of the aromatic ring and formation of CQLA, followed by the release of chloride ions. The aromatic intermediates undergo an oxidative ring opening to form aliphatic carboxylic acids among them oxamic and oxalic acids and release of organic nitrogen as nitrates and ammonium ions. The

latter are slowly mineralized into CO<sub>2</sub>.

#### 4. Conclusion

This work demonstrates that electro-Fenton oxidation using carbon felt cathode and BDD anode accomplished the complete removal of chloroquine drug, CLQ, and 92% TOC removal under optimized operational conditions (0.05 M Na<sub>2</sub>SO<sub>4</sub>, pH = 3.0, j = 60 mA/cm<sup>2</sup>, O<sub>2</sub> flow rate = 80 mL/min, T = 25 °C, stirring = 300 rpm). The efficiency of electro-Fenton oxidation is in good correlation with the generation of H<sub>2</sub>O<sub>2</sub> by electrochemical reduction of O<sub>2</sub> at carbon felt cathode. Higher H<sub>2</sub>O<sub>2</sub> generation was achieved with electro-Fenton-BDD compared to electro-Fenton-Pt and anodic oxidation using Pt and BDD anodes. The most cost-effective H<sub>2</sub>O<sub>2</sub> generation was obtained at pH = 3, j = 60 mA/cm<sup>2</sup>, O<sub>2</sub> flow rate = 80 mL/min using carbon felt cathode and BDD anode. The kinetics of CLQ depletion follows a pseudo-first order reaction for all the operational conditions. The rate constant decreases with the increase of CLQ concentration and pH; however it increases with the increase of current density, and Fe<sup>2+</sup> dose. The increase of current density up to 60 mA/cm<sup>2</sup> enhances CLQ degradation, but higher current densities than 60 mA/cm<sup>2</sup> increases the specific electrical charge consumption. The addition of 10 mg/L Fe<sup>2+</sup> was optimal to deplete CLQ in a reasonable time and without formation of Fe(OH)<sub>3</sub> precipitate. HPLC analysis identified some of CLQ degradation intermediates including CQLA as an aromatic intermediate and OMA and OAA as carboxylic acids. The mineralization of CLQ drug was confirmed by the release of chloride and inorganic nitrogen ions (nitrates and ammonium). CLQ degradation by electro-Fenton oxidation involves several oxidation pathways including the mediated oxidation by HO• radicals produced in solution by catalytic decomposition of H<sub>2</sub>O<sub>2</sub> with Fe<sup>2+</sup>, the mediated oxidation by HO• and sulfate radicals electrogenerated at the surface of BDD anode, mediated oxidation by strong oxidants generated by anodic oxidation of electrolyte (persulfates), and direct electrochemical oxidation of CLQ and its intermediates at the

surface of BDD anode.

### CRedit authorship contribution statement

**Sondos Midassi:** Investigation, Data curation, Writing - original draft. **Ahmed Bedoui:** Data curation, Supervision, Resources, Project administration. **Nasr Bensalah:** Conceptualization, Supervision, Validation, Writing - review & editing.

### Declaration of competing interest

The authors declare that they have no known competing financial interests or personal relationships that could have appeared to influence the work reported in this paper.

### Appendix A. Supplementary data

Supplementary data to this article can be found online at <https://doi.org/10.1016/j.chemosphere.2020.127558>.

### References

- Ahmad, I., Ahmed, S., Anwar, Z., Sheraz, M.A., Sikorski, M., 2016. Photostability and photostabilization of drugs and drug products. *Int. J. Photoenergy*. <https://doi.org/10.1155/2016/8135608>.
- Ahmed, B., Limem, E., Abdel-Wahab, A., Nasr, B., 2011. Photo-Fenton treatment of actual agro-industrial wastewaters. *Ind. Eng. Chem. Res.* <https://doi.org/10.1021/ie200266d>.
- Ahmed, B., Mohamed, H., Limem, E., Nasr, B., 2009. Degradation and mineralization of organic pollutants contained in actual pulp and paper mill wastewaters by a UV/H<sub>2</sub>O<sub>2</sub> process. *Ind. Eng. Chem. Res.* <https://doi.org/10.1021/ie801755u>.
- Asghar, A., Raman, A.A.A., Daud, W.M.A.W., 2015a. Advanced oxidation processes for in-situ production of hydrogen peroxide/hydroxyl radical for textile wastewater treatment: a review. *J. Clean. Prod.* <https://doi.org/10.1016/j.jclepro.2014.09.010>.
- Asghar, A., Raman, A.A.A., Daud, W.M.A.W., 2015b. Advanced oxidation processes for in-situ production of hydrogen peroxide/hydroxyl radical for textile wastewater treatment: a review. *J. Clean. Prod.* <https://doi.org/10.1016/j.jclepro.2014.09.010>.
- Babunpusami, A., Muthukumar, K., 2014a. A review on Fenton and improvements to the Fenton process for wastewater treatment. *J. Environ. Chem. Eng.* <https://doi.org/10.1016/j.jece.2013.10.011>.
- Babunpusami, A., Muthukumar, K., 2014b. A review on Fenton and improvements to the Fenton process for wastewater treatment. *J. Environ. Chem. Eng.* <https://doi.org/10.1016/j.jece.2013.10.011>.
- Badmus, K.O., Tijani, J.O., Massima, E., Petrik, L., 2018. Treatment of persistent organic pollutants in wastewater using hydrodynamic cavitation in synergy with advanced oxidation process. *Environ. Sci. Pollut. Res.* <https://doi.org/10.1007/s11356-017-1171-z>.
- Bensalah, N., Bedoui, A., Chellam, S., Abdel-Wahab, A., 2013. Electro-Fenton treatment of photographic processing wastewater. *Clean* 41. <https://doi.org/10.1002/clen.201200521>.
- Bensalah, N., Chair, K., Bedoui, A., 2018. Efficient degradation of tannic acid in water by UV/H<sub>2</sub>O<sub>2</sub> process. *Sustain. Environ. Res.* <https://doi.org/10.1016/j.serj.2017.04.004>.
- Bensalah, N., Dbira, S., Bedoui, A., 2015. The contribution of mediated oxidation mechanisms in the electrolytic degradation of cyanuric acid using diamond anodes. *J. Environ. Sci. (China)* 45. <https://doi.org/10.1016/j.jes.2015.10.015>.
- Boczkaj, G., Fernandes, A., 2017. Wastewater treatment by means of advanced oxidation processes at basic pH conditions: a review. *Chem. Eng. J.* <https://doi.org/10.1016/j.cej.2017.03.084>.
- Bokare, A.D., Choi, W., 2014. Review of iron-free Fenton-like systems for activating H<sub>2</sub>O<sub>2</sub> in advanced oxidation processes. *J. Hazard Mater.* <https://doi.org/10.1016/j.jhazmat.2014.04.054>.
- Borrás, N., Arias, C., Oliver, R., Brillas, E., 2013. Anodic oxidation, electro-Fenton and photoelectro-Fenton degradation of cyanazine using a boron-doped diamond anode and an oxygen-diffusion cathode. *J. Electroanal. Chem.* <https://doi.org/10.1016/j.jelechem.2012.11.012>.
- Brillas, E., Martínez-Huitle, C.A., 2009. Applied Catalysis B : environmental Decontamination of wastewaters containing synthetic organic dyes by electrochemical methods : a general review. *Appl. Catal. B Environ.* <https://doi.org/10.1016/j.apcatb.2008.09.017>.
- Brillas, E., Sirés, I., Oturan, M.A., 2009. Electro-fenton process and related electrochemical technologies based on fenton's reaction chemistry. *Chem. Rev.* <https://doi.org/10.1021/cr900136g>.
- Cheng, M., Zeng, G., Huang, D., Lai, C., Xu, P., Zhang, C., Liu, Y., 2016. Hydroxyl radicals based advanced oxidation processes (AOPs) for remediation of soils contaminated with organic compounds: a review. *Chem. Eng. J.* <https://doi.org/10.1016/j.cej.2015.09.001>.
- Clarizia, L., Russo, D., Di Somma, I., Marotta, R., Andreozzi, R., 2017. Homogeneous photo-Fenton processes at near neutral pH: a review. *Appl. Catal. B Environ.* <https://doi.org/10.1016/j.apcatb.2017.03.011>.
- Coelho, A.S., Chagas, C.E.P., de Pádua, R.M., Pianetti, G.A., Fernandes, C., 2017. A comprehensive stability-indicating HPLC method for determination of chloroquine in active pharmaceutical ingredient and tablets: identification of oxidation impurities. *J. Pharmaceut. Biomed. Anal.* <https://doi.org/10.1016/j.jpba.2017.06.023>.
- Cortegiani, A., Ingoglia, G., Ippolito, M., Giarratano, A., Einav, S., 2020. A systematic review on the efficacy and safety of chloroquine for the treatment of COVID-19. *J. Crit. Care.* <https://doi.org/10.1016/j.jccr.2020.03.005>.
- Dbira, S., Bedoui, A., Bensalah, N., 2014. Investigations on the degradation of triazine herbicides in water by photo-fenton process. *Am. J. Anal. Chem.* <https://doi.org/10.4236/ajac.2014.58059>.
- Dbira, S., Bensalah, N., Bedoui, A., Cañizares, P., Rodrigo, M.A., 2015. Treatment of synthetic urine by electrochemical oxidation using conductive-diamond anodes. *Environ. Sci. Pollut. Res.* <https://doi.org/10.1007/s11356-014-3831-6>.
- de Freitas Araújo, K.C., da Silva, D.R., dos Santos, E.V., Varela, H., Martínez-Huitle, C.A., 2020. Investigation of persulfate production on BDD anode by understanding the impact of water concentration. *J. Electroanal. Chem.* <https://doi.org/10.1016/j.jelechem.2020.113927>.
- Deng, Y., Zhao, R., 2015. Advanced oxidation processes (AOPs) in wastewater treatment. *Curr. Pollut. Reports.* <https://doi.org/10.1007/s40726-015-0015-z>.
- Devaux, C.A., Rolain, J.-M., Colson, P., Raoult, D., 2020. New insights on the antiviral effects of chloroquine against coronavirus: what to expect for COVID-19? *Int. J. Antimicrob. Agents.* <https://doi.org/10.1016/j.ijantimicag.2020.105938>.
- Doddaga, S., Peddakonda, R., 2013. Chloroquine-N-oxide, a major oxidative degradation product of chloroquine: identification, synthesis and characterization. *J. Pharmaceut. Biomed. Anal.* <https://doi.org/10.1016/j.jpba.2013.04.004>.
- Eisenberg, G.M., 1943. Colorimetric determination of hydrogen peroxide. *Ind. Eng. Chem. - Anal. Ed.* <https://doi.org/10.1021/i560117a011>.
- El-Ghenymy, A., Centellas, F., Rodríguez, R.M., Cabot, P.L., Garrido, J.A., Sirés, I., Brillas, E., 2015. Comparative use of anodic oxidation, electro-Fenton and photoelectro-Fenton with Pt or boron-doped diamond anode to decolorize and mineralize Malachite Green oxalate dye. *Electrochim. Acta.* <https://doi.org/10.1016/j.electacta.2015.09.078>.
- El-Ghenymy, A., Garrido, J.A., Centellas, F., Arias, C., Cabot, P.L., Rodríguez, R.M., Brillas, E., 2012. Electro-fenton and photoelectro-fenton degradation of sulfanilic acid using a boron-doped diamond anode and an air diffusion cathode. *J. Phys. Chem.* <https://doi.org/10.1021/jp300442y>.
- Escalona-Durán, F., Ribeiro da Silva, D., Martínez-Huitle, C.A., Villegas-Guzman, P., 2020. The synergic persulfate-sodium dodecyl sulfate effect during the electro-oxidation of caffeine using active and non-active anodes. *Chemosphere.* <https://doi.org/10.1016/j.chemosphere.2020.126599>.
- Frosch, A.E., Venkatesan, M., Laufer, M.K., 2011. Patterns of chloroquine use and resistance in sub-Saharan Africa: a systematic review of household survey and molecular data. *Malar. J.* <https://doi.org/10.1186/1475-2875-10-116>.
- Furst, D.E., 1996. Pharmacokinetics of hydroxychloroquine and chloroquine during treatment of rheumatic diseases. *Lupus.* <https://doi.org/10.1177/0961203396005001041>.
- Gągól, M., Przyjazny, A., Boczkaj, G., 2018. Wastewater treatment by means of advanced oxidation processes based on cavitation – a review. *Chem. Eng. J.* <https://doi.org/10.1016/j.cej.2018.01.049>.
- Gao, J., Tian, Z., Yang, X., 2020. Breakthrough: chloroquine phosphate has shown apparent efficacy in treatment of COVID-19 associated pneumonia in clinical studies. *Biosci. Trends.* <https://doi.org/10.5582/bst.2020.01047>.
- Gao, Y., Zhu, W., Wang, C., Zhao, X., Shu, M., Zhang, J., Bai, H., 2020. Enhancement of oxygen reduction on a newly fabricated cathode and its application in the electro-Fenton process. *Electrochim. Acta.* <https://doi.org/10.1016/j.electacta.2019.135206>.
- García-Segura, S., Brillas, E., 2011. Mineralization of the recalcitrant oxalic and oxamic acids by electrochemical advanced oxidation processes using a boron-doped diamond anode. *Water Res.* <https://doi.org/10.1016/j.watres.2011.03.017>.
- Gligorovski, S., Strekowski, R., Barbati, S., Vione, D., 2015. Environmental implications of hydroxyl radicals (•OH). *Chem. Rev.* <https://doi.org/10.1021/cr500310b>.
- Gong, Y., Li, J., Zhang, Y., Zhang, M., Tian, X., Wang, A., 2016. Partial degradation of levofloxacin for biodegradability improvement by electro-Fenton process using an activated carbon fiber felt cathode. *J. Hazard Mater.* <https://doi.org/10.1016/j.jhazmat.2015.10.064>.
- Groenen Serrano, K., 2018. Indirect electrochemical oxidation using hydroxyl radical, active chlorine, and peroxodisulfate. In: *Electrochemical Water and Wastewater Treatment.* <https://doi.org/10.1016/b978-0-12-813160-2.00006-7>.
- Guinea, E., Garrido, J.A., Rodríguez, R.M., Cabot, P.L., Arias, C., Centellas, F., Brillas, E., 2010. Degradation of the fluoroquinolone enrofloxacin by electrochemical advanced oxidation processes based on hydrogen peroxide electrogeneration. *Electrochim. Acta.* <https://doi.org/10.1016/j.electacta.2009.11.040>.
- Hou, C., Shen, J., Jiang, X., Zhang, D., Sun, X., Li, J., Han, W., Liu, X., Wang, L., 2018. Enhanced anoxic biodegradation of pyridine coupled to nitrification in an inner loop anoxic/oxic-dynamic membrane bioreactor (A/O-DMBR). *Bioresour. Technol.* <https://doi.org/10.1016/j.biortech.2018.07.105>.
- Howard, B., 2007. Hydroxychloroquine. In: *XPharm: the Comprehensive Pharmacology Reference.* <https://doi.org/10.1016/B978-0-08055232-3.61897-5>.
- Huong Le, T.X., Bechelany, M., Cretin, M., 2017. Carbon felt based-electrodes for energy and environmental applications: a review. *Carbon N. Y.* <https://doi.org/10.1016/j.carbon.2017.06.078>.
- Jiang, C., Pang, S., Ouyang, F., Ma, J., Jiang, J., 2010. A new insight into Fenton and

- Fenton-like processes for water treatment. *J. Hazard Mater.* <https://doi.org/10.1016/j.jhazmat.2009.09.125>.
- Kanakaraju, D., Glass, B.D., Oelgemöller, M., 2018. Advanced oxidation process-mediated removal of pharmaceuticals from water: a review. *J. Environ. Manag.* <https://doi.org/10.1016/j.jenvman.2018.04.103>.
- Karim, E.I.A., Ibrahim, K.E.E., Abdelrahman, A.N., Fell, A.F., 1994. Photodegradation studies on chloroquine phosphate by high-performance liquid chromatography. *J. Pharmaceut. Biomed. Anal.* [https://doi.org/10.1016/0731-7085\(93\)E0026-J](https://doi.org/10.1016/0731-7085(93)E0026-J).
- Klassen, N.V., Marchington, D., McGowan, H.C.E., 1994. H<sub>2</sub>O<sub>2</sub> determination by the I<sub>3</sub><sup>-</sup> method and by KMnO<sub>4</sub> titration. *Anal. Chem.* <https://doi.org/10.1021/ac00090a020>.
- Lee, S.J., Silverman, E., Bargman, J.M., 2011. The role of antimalarial agents in the treatment of SLE and lupus nephritis. *Nat. Rev. Nephrol.* <https://doi.org/10.1038/nrneph.2011.150>.
- Marselli, B., García-Gomez, J., Michaud, P., Rodrigo, M.A., Comninellis, C., 2003. Electrogeneration of hydroxyl radicals on boron-doped diamond electrodes. *J. Electrochem. Soc.* <https://doi.org/10.1149/1.1553790>.
- Martínez-Huitle, C.A., Panizza, M., 2018. Electrochemical oxidation of organic pollutants for wastewater treatment. *Curr. Opin. Electrochem.* <https://doi.org/10.1016/j.coelec.2018.07.010>.
- Michaud, P.A., Mahé, E., Haenni, W., Perret, A., Comninellis, C., 2000. Preparation of peroxodisulfuric acid using boron-doped diamond thin film electrodes. *Electrochim. Solid State Lett.* <https://doi.org/10.1149/1.1390963>.
- Michaud, P.A., Panizza, M., Ouattara, L., Diaco, T., Foti, G., Comninellis, C., 2003. Electrochemical oxidation of water on synthetic boron-doped diamond thin film anodes. *J. Appl. Electrochem.* <https://doi.org/10.1023/A:1024084924058>.
- Miklos, D.B., Remy, C., Jekel, M., Linden, K.G., Drewes, J.E., Hübner, U., 2018. Evaluation of advanced oxidation processes for water and wastewater treatment – a critical review. *Water Res.* <https://doi.org/10.1016/j.watres.2018.03.042>.
- Moreira, F.C., Garcia-Segura, S., Vilar, V.J.P., Boaventura, R.A.R., Brillas, E., 2013. Decolorization and mineralization of Sunset Yellow FCF azo dye by anodic oxidation, electro-Fenton, UVA photoelectro-Fenton and solar photoelectro-Fenton processes. *Appl. Catal. B Environ.* <https://doi.org/10.1016/j.apcatb.2013.03.023>.
- Nasr, B., Abdellatif, G., Cañizares, P., Sáez, C., Lobato, J., Rodrigo, M.A., 2005. Electrochemical oxidation of hydroquinone, resorcinol, and catechol on boron-doped diamond anodes. *Environ. Sci. Technol.* <https://doi.org/10.1021/es0500660>.
- Nord, K., Karlsen, J., Tønnesen, H.H., 1991. Photochemical stability of biologically active compounds. IV. Photochemical degradation of chloroquine. *Int. J. Pharm.* [https://doi.org/10.1016/0378-5173\(91\)90375-X](https://doi.org/10.1016/0378-5173(91)90375-X).
- Özcan, A., Şahin, Y., Savaş Kopalal, A., Oturan, M.A., 2008. Carbon sponge as a new cathode material for the electro-Fenton process: comparison with carbon felt cathode and application to degradation of synthetic dye basic blue 3 in aqueous medium. *J. Electroanal. Chem.* <https://doi.org/10.1016/j.jelechem.2008.01.002>.
- Panizza, M., Brillas, E., Comninellis, C., 2008. Application of boron-doped diamond electrodes for wastewater treatment. *J. Environ. Eng. Manag.*
- Peralta, E., Roa, G., Hernandez-Servin, J.A., Romero, R., Balderas, P., Natividad, R., 2014. Hydroxyl Radicals quantification by UV spectrophotometry. *Electrochim. Acta.* <https://doi.org/10.1016/j.electacta.2014.02.047>.
- Pereira, G.F., El-Ghenymy, A., Thiam, A., Carlesi, C., Eguiluz, K.I.B., Salazar-Banda, G.R., Brillas, E., 2016. Effective removal of Orange-G azo dye from water by electro-Fenton and photoelectro-Fenton processes using a boron-doped diamond anode. *Separ. Purif. Technol.* <https://doi.org/10.1016/j.seppur.2016.01.029>.
- Pham, A.L.T., Doyle, F.M., Sedlak, D.L., 2012. Kinetics and efficiency of H<sub>2</sub>O<sub>2</sub> activation by iron-containing minerals and aquifer materials. *Water Res.* <https://doi.org/10.1016/j.watres.2012.09.020>.
- Pignatello, J.J., Oliveros, E., MacKay, A., 2006. Advanced oxidation processes for organic contaminant destruction based on the fenton reaction and related chemistry. *Crit. Rev. Environ. Sci. Technol.* <https://doi.org/10.1080/10643380500326564>.
- Pinheiro, V.S., Paz, E.C., Aveiro, L.R., Parreira, L.S., Souza, F.M., Camargo, P.H.C., Santos, M.C., 2019. Mineralization of paracetamol using a gas diffusion electrode modified with ceria high aspect ratio nanostructures. *Electrochim. Acta.* <https://doi.org/10.1016/j.electacta.2018.10.097>.
- Price, R.N., von Seidlein, L., Valecha, N., Nosten, F., Baird, J.K., White, N.J., 2014. Global extent of chloroquine-resistant Plasmodium vivax: a systematic review and meta-analysis. *Lancet Infect. Dis.* [https://doi.org/10.1016/S1473-3099\(14\)70855-2](https://doi.org/10.1016/S1473-3099(14)70855-2).
- Rice, E.W., Baird, R.B., Eaton, A.D., 2017. 4500-Cl chlorine (residual). *Stand. Methods exam. Water wastewater.* <https://doi.org/10.2105/SMWW.2882.078>.
- Ruiz, E.J., Hernández-Ramírez, A., Peralta-Hernández, J.M., Arias, C., Brillas, E., 2011. Application of solar photoelectro-Fenton technology to azo dyes mineralization: effect of current density, Fe<sup>2+</sup> and dye concentrations. *Chem. Eng. J.* <https://doi.org/10.1016/j.cej.2011.03.004>.
- Schrezenmeier, E., Dörner, T., 2020. Mechanisms of action of hydroxychloroquine and chloroquine: implications for rheumatology. *Nat. Rev. Rheumatol.* <https://doi.org/10.1038/s41584-020-0372-x>.
- Serrano, K., Michaud, P.A., Comninellis, C., Savall, A., 2002. Electrochemical preparation of peroxodisulfuric acid using boron doped diamond thin film electrodes. *Electrochim. Acta.* [https://doi.org/10.1016/S0013-4686\(02\)00688-6](https://doi.org/10.1016/S0013-4686(02)00688-6).
- Shemer, H., Linden, K.G., 2006. Degradation and by-product formation of diazinon in water during UV and UV/H<sub>2</sub>O<sub>2</sub> treatment. *J. Hazard Mater.* <https://doi.org/10.1016/j.jhazmat.2005.12.028>.
- Singh, R., Adhikari, D.R., Patil, B.P., Talathi, N.R., Hanamshetti, S.R., Joshi, R.M., 2011. Amoebic liver abscess: an appraisal. *Int. Surg.* <https://doi.org/10.9738/CC9.1>.
- Singh, S., Chaudhary, P., Saxena, N., Khandelwal, S., Poddar, D.D., Biswal, U.C., 2013. Treatment of liver abscess: prospective randomized comparison of catheter drainage and needle aspiration. *Ann. Gastroenterol.*
- Tayo, L.L., Caparanga, A.R., Doma, B.T., Liao, C.H., 2018. A review on the removal of pharmaceutical and personal care products (PPCPs) using advanced oxidation processes. *J. Adv. Oxid. Technol.* <https://doi.org/10.26802/jaots.2017.0079>.
- Teymori, M., Khorsandi, H., Aghapour, A.A., Jafari, S.J., Maleki, R., 2020. Electro-Fenton method for the removal of Malachite Green: effect of operational parameters. *Appl. Water Sci.* <https://doi.org/10.1007/s13201-019-1123-5>.
- Vallejo, M., Fresnedo San Román, M., Ortiz, I., Irabien, A., 2015. Overview of the PCDD/Fs degradation potential and formation risk in the application of advanced oxidation processes (AOPs) to wastewater treatment. *Chemosphere.* <https://doi.org/10.1016/j.chemosphere.2014.05.077>.
- Wang, J.L., Xu, L.J., 2012. Advanced oxidation processes for wastewater treatment: formation of hydroxyl radical and application. *Crit. Rev. Environ. Sci. Technol.* <https://doi.org/10.1080/10643389.2010.507698>.
- Wang, Y., Zhou, W., Gao, J., Ding, Y., Kou, K., 2019. Oxidative modification of graphite felts for efficient H<sub>2</sub>O<sub>2</sub> electrogeneration: enhancement mechanism and long-term stability. *J. Electroanal. Chem.* <https://doi.org/10.1016/j.jelechem.2018.11.051>.
- Xiang, Q., Yu, J., Wong, P.K., 2011. Quantitative characterization of hydroxyl radicals produced by various photocatalysts. *J. Colloid Interface Sci.* <https://doi.org/10.1016/j.jcis.2011.01.093>.
- Yang, W., Zhou, M., Cai, J., Liang, L., Ren, G., Jiang, L., 2017. Ultrahigh yield of hydrogen peroxide on graphite felt cathode modified with electrochemically exfoliated graphene. *J. Mater. Chem.* <https://doi.org/10.1039/c7ta01534h>.
- Yu, F., Zhou, M., Yu, X., 2015. Cost-effective electro-Fenton using modified graphite felt that dramatically enhanced on H<sub>2</sub>O<sub>2</sub> electro-generation without external aeration. *Electrochim. Acta.* <https://doi.org/10.1016/j.electacta.2015.02.166>.
- Yu, F., Zhou, M., Zhou, L., Peng, R., 2014. A novel electro-fenton process with H<sub>2</sub>O<sub>2</sub> generation in a rotating disk reactor for organic pollutant degradation. *Environ. Sci. Technol. Lett.* <https://doi.org/10.1021/ez500178p>.
- Zhang, Z., Meng, H., Wang, Y., Shi, L., Wang, X., Chai, S., 2018. Fabrication of graphene@graphite-based gas diffusion electrode for improving H<sub>2</sub>O<sub>2</sub> generation in Electro-Fenton process. *Electrochim. Acta.* <https://doi.org/10.1016/j.electacta.2017.11.048>.
- Zhou, L., Hu, Z., Zhang, C., Bi, Z., Jin, T., Zhou, M., 2013. Electrogeneration of hydrogen peroxide for electro-Fenton system by oxygen reduction using chemically modified graphite felt cathode. *Separ. Purif. Technol.* <https://doi.org/10.1016/j.seppur.2013.03.038>.
- Zöllig, H., Fritzsche, C., Morgenroth, E., Udert, K.M., 2015. Direct electrochemical oxidation of ammonia on graphite as a treatment option for stored source-separated urine. *Water Res.* <https://doi.org/10.1016/j.watres.2014.11.031>.